Electronic Supporting Information

Cellulosic nanocomposite filaments for an ionic strength sensor with ultrahigh precision and sensitivity

Yuying Kong,[a] *Hui Mao,*[a] *Zihuan Zhang,*[a] *Junqi Gao,*[a] *Xiao Han,*[a] *Wen-Jun Wang,*[a,b] *Khak Ho Lim,*[b] *Xuan Yang*[a,b*]

[a.] State Key Laboratory of Chemical Engineering, Key Laboratory of Biomass Chemical Engineering of Ministry of Education, College of Chemical and Biological Engineering, Zhejiang University, Hangzhou 310027, P.R. China;

[b] Institute of Zhejiang University. Quzhou, 324000, P.R. China.

* Corresponding author email: xuan.yang@zju.edu.cn.

Preparation of TEMPO-Fibers

Starting from white pine chips, a mild peracetic acid (PAA) delignification was carried out [Macromolecules, 2021, 54, 4443–4452; ACS Nano, 2020, 14, 724–735]. The PAA solution had a concentration of 4 wt%, and the pH was adjusted to 4.6 by adding NaOH. The reaction was performed at a temperature of 85 °C for 1 hour, and then the treated wood chips were thoroughly washed using deionized water. Then another 3-4 rounds of such identical PAA treatment were carried out, until the chips showed a pure white color. The treated chips were then subjected to a classic TEMPO oxidation under basic conditions [Biomacromolecules, 2006, 7, 1687–1691]. TEMPO (0.1 mmol g^{-1} dry fiber) and sodium bromide (1 mmol g^{-1} dry fiber) were dissolved in deionized water and mixed with delignified chips, followed by the addition of NaClO (10 mmol g^{-1} dry fiber). To maintain the pH of 10.5 during the reaction process, a 20 wt% sodium hydroxide solution was employed. After 1.5 hours, the washing product was filtered using deionized water until the pH of the filtrate reached 7. The final treated chips were easily processed into individual TEMPO-Fibers through gentle mechanical stirring/shaking.

Preparation of TEMPO-CNFs

The never dried TEMPO-Fibers were fibrillated into CNFs using a kitchen blender (Joyoung Y921, China) at 30,000 rpm for 15 min, during which deionized water was slowly added until a desired concentration (0.4 wt%) was reached.

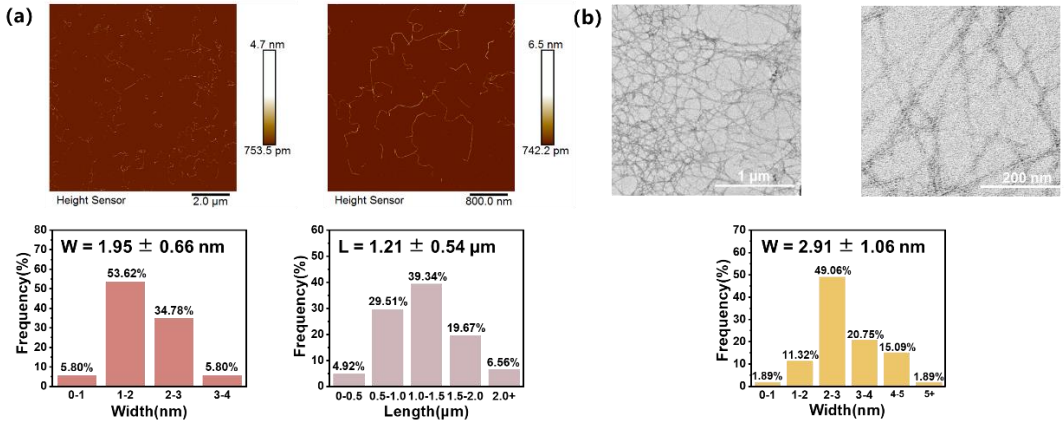

Fig. S1. AFM (a) and TEM (b) images of CNFs and the corresponding measured width and length.

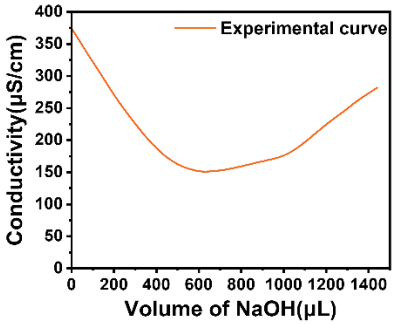

Fig. S2. The conductometric curve for the TEMPO-CNFs. The content of the carboxyl groups is determined to be 460 ± 30 μmol g^{-1}.

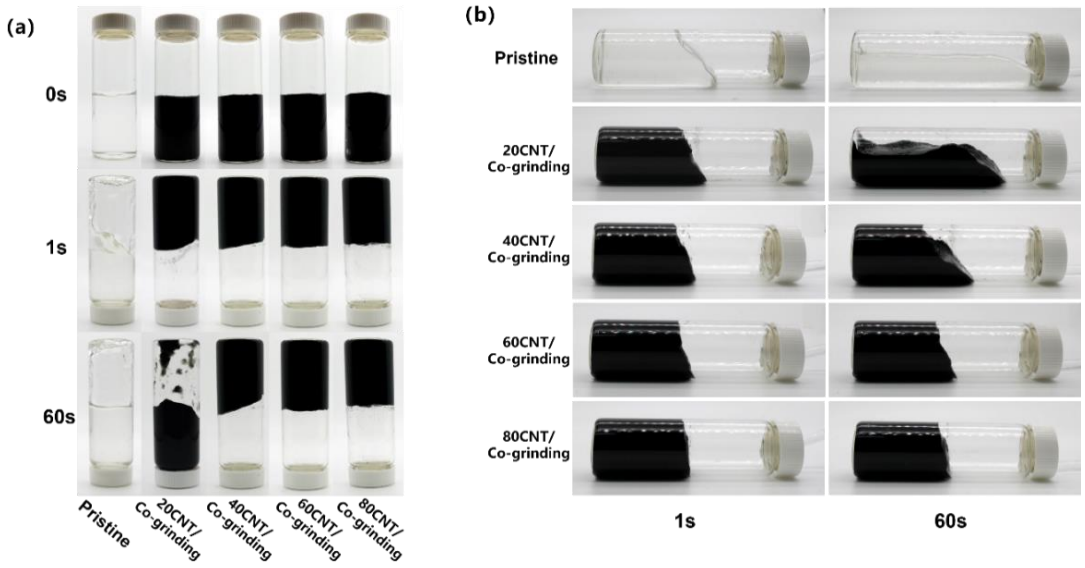

Fig. S3. Photos of pristine and composite suspensions with varying CNT concentrations, along with their corresponding (a) inverted flowability and (b) virtual flowability at 1 and 60 s.

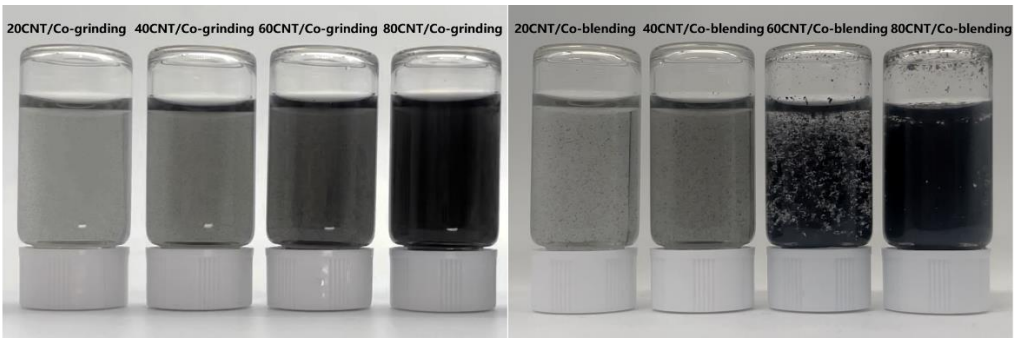

Fig. S4. Photos of diluted composite suspensions (~ 0.001 wt%) with varying CNT concentrations.

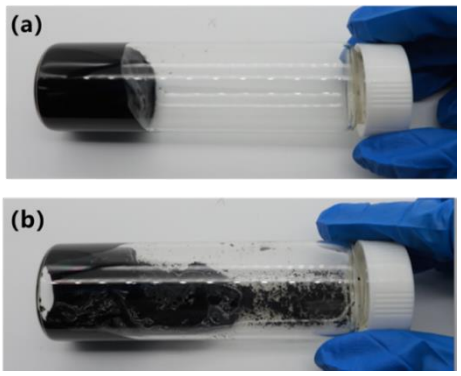

Fig. S5. Comparation of composite suspensions prepared using (a) co-grinding and (b) co-blending methods. Note that photos were taken after the suspensions had been stored for 30 days to assess their stability.

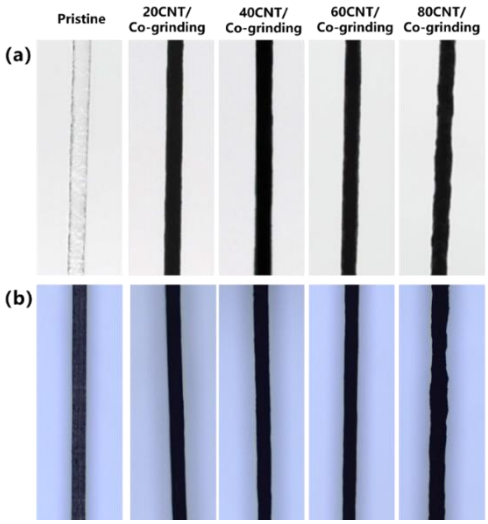

Fig. S6. Images of pristine and composite filaments with varying CNT concentrations in (a) wet and (b) dry states.

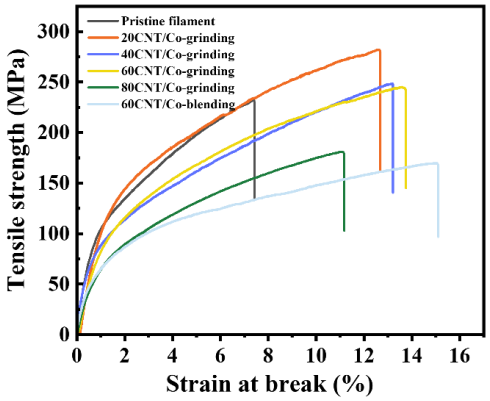

Fig. S7. Stress-strain curves of composite filaments prepared by co-grinding and co-blending suspensions with varying CNT concentrations. The detailed results are listed in the Table S1.

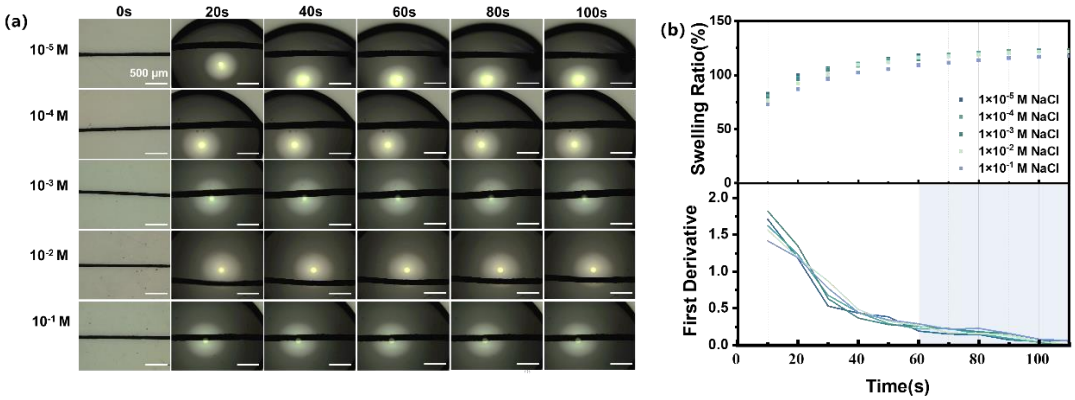

Fig. S8 The confined capillary swelling behavior of 60CNT/Co-grinding filament sensors when detecting NaCl solutions with concentrations ranging from 10^{-5} to 10^{-1} M: (a) optical images of the swelling, (b) the swelling ratio, and the corresponding first derivative curves of the swelling ratio. Note that the first derivative remains relatively stable after 60 seconds.

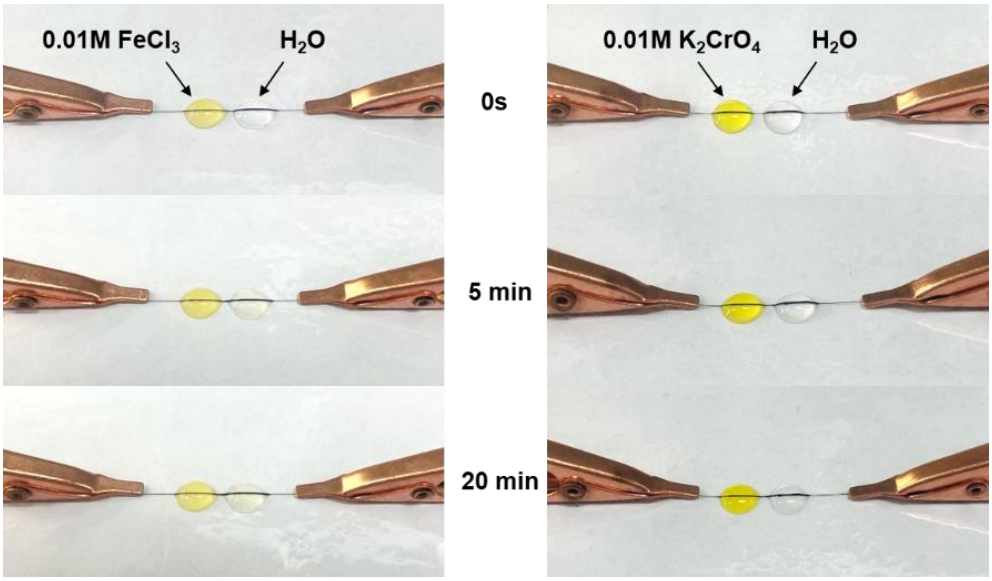

Fig. S9. Visualization of ion transportation when detecting salt solutions with color.

Table S1. Mechanical properties of pristine and composite filaments prepared by co-grinding and co-blending suspensions with varying CNT concentrations.

	Young's Modulus (GPa)	Tensile Strength (MPa)	Strain (%)
Pristine filament	10.62 ± 1.02	231.44 ± 15.68	7.48 ± 0.58
20CNT/Co-grinding	15.09 ± 1.50	273.41 ± 18.55	12.11 ± 2.07
40CNT/Co-grinding	13.01 ± 1.68	235.26 ± 15.35	14.53 ± 2.40
60CNT/Co-grinding	12.54 ± 1.84	229.12 ± 19.20	12.65 ± 2.66
80CNT/Co-grinding	10.33 ± 1.61	183.30 ± 10.05	10.14 ± 1.33
60CNT/Co-blending	11.03 ± 1.61	163.45 ± 16.88	14.18 ± 2.45

Table S2. Normalized resistance and conductivity of composite filaments prepared by co-grinding and co-blending suspensions with varying CNT concentrations.

	Normalized Resistance (Ω)	Conductivity (S cm^{-1})
20CNT/Co-grinding	1822.62 ± 109.67	25.60 ± 3.20
40CNT/Co-grinding	223.30 ± 14.29	187.67 ± 17.48
60CNT/Co-grinding	77.61 ± 4.79	441.15 ± 35.42
80CNT/Co-grinding	144.23 ± 9.22	141.95 ± 8.36
60CNT/Co-blending	120.06 ± 7.63	233.20 ± 14.78

Table S3. Mechanical properties and conductivity of different types of cellulose/CNT composites including films/nanopapers and filaments.

Reference	Materials	Form	Mechanical Properties		Conductivity ($S\ cm^{-1}$)
			Tensile Strength (MPa)	Young's Modulus (GPa)	
Our work	**CNF/CNT**	**filament**	**229.12 ± 19.20**	**12.54 ± 1.84**	**441.15 ± 35.42**
			273.41 ± 18.55	**15.09 ± 1.50**	**25.60 ± 3.20**
Rahatekar et al, 2009 (REF 31)	Cellulose/CNT	filament	179 ± 24	13.0 ± 0.2	30.75
			257 ± 9	14.9 ± 1.3	0.19
Wan et al, 2019 (REF 32)	CNF/CNT	filament	223.2 ± 8.54	16.02 ±0.36	86.43 ± 3.99
			246.96 ±5.07	11.05 ±0.68	4.98 ± 0.32
Cho et al, 2019 (REF 33)	Tunicate Cellulose/CNF	filament	162	/	13
			240	11-19	2.43
Li et al, 2017 (REF 52)	CNF/CNT	filament	247 ± 5	/	216.7 ± 10
Zhang et al, 2020 (REF 53)	CNF/CNT	filament	125 ± 13	6.3 ± 2	20.56 ± 2.3
			149 ± 17	7.3 ± 3	0.096 ± 0.03
Ma et al, 2021 (REF 54)	Cellulose/CNT	filament	114 ± 5	6.1 ± 1	12.74
			185 ± 9	10.6 ± 1	0.64
Huang et al, 2015 (REF 30)	Cellulose/CNT	film	50.5	3.8	0.072
			77.8	4.6	1E-6
Salajkova et al, 2013 (REF 47)	CNF/CNT	nanopaper	66.2 ± 8.3	2.6 ± 0.16	0.01
			177 ± 21.0	9.34 ± 0.57	0.001
Hajian et al, 2019 (REF 48)	CNF/CNT	nanopaper	100	7.6 ± 0.5	115 ± 5
			253	13.7 ± 0.3	0.95
Koga et al, 2013 (REF 49)	CNF/CNT	film	70	9	10
			250	12	0.001
Hamedi et al, 2014 (REF 50)	CNF/CNT	film	220	14	207
			307 ± 6	13.3 ± 0.3	0.03
Zhang et al, 2018 (REF 51)	CNF/CNT	film	25	/	30.24
			48	/	23.56

Note the references in this table is linked to the main article.

Table S4. The fitting parameters of ionic strength sensing performance in different NaCl concentration ranges.

Wetting Curve Intervals	Fitted Equation	Pearson's R	R-Square
I (10^{-5}-10^{-4} M)	y=11547.9x+0.26	0.99929	0.99858
II (10^{-4}-10^{-3} M)	y=858.9x+1.35	0.99944	0.99888
III (10^{-3}-10^{-2} M)	y=148.6x+2.06	0.99997	0.99994
IV (10^{-2}-10^{-1} M)	y=20.1x+3.29	0.99942	0.99885

Table S5. The hydrated radius of different cations [Bioelectrochemistry and bioenergetics, 1997, 42(2): 153-160; Thin Solid Films, 2009, 517(5): 1616-1619] and the $\Delta R/R_0$ at 1 min of wetting.

Cation Type (Anion: Cl^-)	Hydrated Radius (pm)	$\Delta R/R_0$-1 min
Na^+	358	3.73 ± 0.12
K^+	331	2.84 ± 0.12
Ca^{2+}	412	2.33 ± 0.13
Fe^{3+}	457	0.85 ± 0.02

Table S6. The hydrated radius of different anions [Bioelectrochemistry and bioenergetics, 1997, 42(2): 153-160; Desalination, 2014, 353: 84-90] and the $\Delta R/R_0$ at 1 min of wetting.

Anion Type (Cation: Na^+)	Hydrated Radius (pm)	$\Delta R/R_0$-1 min
SO_4^{2-}	379	3.76 ± 0.05
NO_3^-	340	3.76 ± 0.09
Cl^-	332	3.73 ± 0.12

Calculation S1. Derivation of ion conductivity formula.

The carriers (here referring to ions) traverse the solution, generating a stable current that achieves equilibrium between the electric field and resistance force. As such, for each ion follows equation S2 accordingly:

$$\vec{F}_E = ze\vec{E} \tag{S2}$$

The resistance force corresponds to the viscous force of the fluid, according to the Stokes Model S3:

$$\overrightarrow{F_f} = -\vec{v}[(3\pi d)\eta] \tag{S3}$$

where $\vec{v}$ is the drift velocity of ions, d is the diameter of the ion and η is the solution viscosity.

According to the definition of current density S4, equation S2 and S3,

$$\vec{j} = \rho\vec{v} = [i]z_i e\vec{v} \tag{S4}$$

equation S5 can be obtained:

$$\vec{j} = \frac{[i](z_i e)^2}{(3\pi \mathrm{d})\eta}\vec{E} \tag{S5}$$

where $[i]$ is the concentration or number density of ions, z_i is the number of charges carried by the ion, and e is the solution viscosity.

The probability ratio between the barrier state and the ground state is the reciprocal of the molecular viscosity and is temperature dependent, which corresponds to equation S6:

$$\emptyset^{-1} = e^{-\frac{G_+^+ - G_0}{KT}} \quad \text{(S6)}$$

where G_+^+ is the highest energy barrier state of the molecule, occurring when it reaches the midpoint between two coordination sites, and G_0 is the minimum energy barrier for a molecule in its ground state, indicating its stable state.

Finally, by combining Maxwell's constitutive equation S7, the solution viscosity of equation S8 and the equation S6,

$$\vec{\boldsymbol{J}} = \sigma\vec{\boldsymbol{E}} \quad \text{(S7)}$$

$$\eta = \eta_0\phi \quad \text{(S8)}$$

the ion conductivity can be derived from equation S9:

$$\sigma = \frac{[i](z_i e)^2}{(3\pi \mathrm{d})\eta} e^{-\frac{E_a}{KT}} \quad \text{(S9)}$$

where $[i]$ is the concentration or number density of ions, Z_i is the number of charges carried by the ion, $E_a = G_+^+ - G_0$ is the activation energy required for transportation, d is the diameter of the ion and η_0 is the solution viscosity at a characteristic temperature ($KT = E_a$) of transportation activation.

Calculation S2. Derivation of the experimental ratio of ion conductivity.

Ion	ΔR/R₀-Ion	ΔR/R₀-Baseline	ΔR/R₀-Ion contribution (Experimental conductivity)	Experimental Ratio
Na^+	3.73	7.27	3.54	$Na^+ : K^+ : Ca^{2+} : Fe^{3+}$ = 1 : 1.25 : 1.39 : 1.81
K^+	2.84		4.43	
Ca^{2+}	2.33		4.94	
Fe^{3+}	0.85		6.42	
SO_4^{2-}	3.76	7.27	3.51	$SO_4^{2-} : NO_3^- : Cl^-$ = 1 : 1 : 1.01
NO_3^-	3.76		3.51	
Cl^-	3.73		3.54	

Note the experimental conductivity presented herein is defined as the difference in $\Delta R/R_0$ between the baseline (corresponding to the purified water) and ions at 1 min.